

J. C. Hillesheim, E. Delabie, H. Meyer, C. F. Maggi, L. Meneses,
E. Poli, and JET Contributors

Direct evidence for zonal flows during formation of the edge pedestal in JET

Enquiries about copyright and reproduction should in the first instance be addressed to the Culham Publications Officer, Culham Centre for Fusion Energy (CCFE), K1/083, Culham Science Centre, Abingdon, Oxfordshire, OX14 3DB, UK. The United Kingdom Atomic Energy Authority is the copyright holder.

Direct evidence for zonal flows during formation of the edge pedestal in JET

J. C. Hillesheim,¹ E. Delabie,² H. Meyer,¹ C. F. Maggi,¹ L. Meneses,³
E. Poli,⁴ and JET Contributors

¹*CCFE, Culham Science Centre, Abingdon, Oxon OX14 3DB, United Kingdom*

²*Oak Ridge National Laboratory, Oak Ridge, Tennessee, USA*

³*Instituto de Plasmas e Fusão Nuclear, Instituto Superior Técnico, Universidade de Lisboa,
Lisboa, Portugal*

⁴*Max-Planck-institut für Plasmaphysik, Garching, Germany*

Direct evidence for zonal flows during formation of the edge pedestal in JET

J. C. Hillesheim,^{1,*} E. Delabie,² H. Meyer,¹ C. F. Maggi,¹ L. Meneses,³ E. Poli,⁴ and JET Contributors*

EUROfusion Consortium JET, Culham Science Centre, Abingdon, OX14 3DB, UK

¹*CCFE, Culham Science Centre, Abingdon, Oxon OX14 3DB, United Kingdom*

²*Oak Ridge National Laboratory, Oak Ridge, Tennessee, USA*

³*Instituto de Plasmas e Fusão Nuclear, Instituto Superior Técnico, Universidade de Lisboa, Lisboa, Portugal*

⁴*Max-Planck-institut für Plasmaphysik, Garching, Germany*

(Dated: October 16, 2015)

High spatial resolution Doppler backscattering measurements in JET have enabled new insights into the development of the edge E_r . We observe fine-scale spatial structures in the edge E_r well with wavenumber $k_r \rho_i \approx 0.4-0.8$, consistent with stationary zonal flows, the characteristics of which vary with density. The zonal flow amplitude and wavelength both decrease with local collisionality, such that the zonal flow $E \times B$ shear increases. Above the minimum of the L-H transition power threshold dependence on density, the zonal flows are present during L-mode and disappear following the H-mode transition, while below the minimum they are reduced below measurable amplitude during L-mode, before the L-H transition.

Introduction – The transition from Low confinement (L-mode) to High confinement (H-mode) in tokamaks occurs due to formation of a transport barrier near the plasma boundary – the pedestal – where the pressure gradient becomes large. This improves global energy confinement by about a factor of two, which is essential for achieving high fusion gain in future devices like ITER. H-mode conditions were discovered in ASDEX more than 30 years ago [1, 2]. It was quickly identified that the development of large shear in the radial electric field plays an important role in the L-H transition [3–6] and that the transition is concurrent with a large drop in the amplitude of long wavelength density fluctuations [7–9]. There has been significant interest in recent years on the role of oscillatory zonal flows (toroidally and poloidally symmetric potential structures, $n=0$, $m=0$, with finite radial wavenumbers) in L-H transition dynamics [10–14] in the form of the geodesic acoustic mode (GAM) and low frequency “limit cycle oscillations” (LCOs). It has also been reported that in some cases the turbulence drive through the measured Reynolds stress is too small to account for the amplitude of LCOs [15]. Many models for the L-H transition have been put forward (for reviews see 16–18; for more recent work see 19–24), but a validated theory has not been identified.

We report high spatial resolution measurements of the radial electric field, E_r , with Doppler backscattering (DBS) in JET, which reveals fine-scale spatial structure in E_r that can be stationary for 100s of ms. This temporal behavior is how zonal flows (ZFs) in tokamaks were predicted [25] and typically appear in non-linear turbulence simulations, rather than the low – but finite – frequency flows reported in experiments [26, 27]. See [28] for a review of ZF physics.

These stationary zonal flows in JET are only observed, so far, in the E_r well and before the L-H transition. ZFs have been predicted to be weak or absent in the pedestal region [29, 30]. It has been well-established that there is a non-monotonic dependence of the L-H transition power threshold, P_{LH} , on density [31–36], which has also been found in JET with the ITER-like W/Be wall [37]. It has been hypothesized that this is related to a decoupling of the ion and electron heat fluxes due to a requirement on only the ion heat flux for the transition [38]; the empirical prediction for the density minimum in [38] agrees reasonably with JET data in some divertor configurations [39]. We report that ZFs are present until the L-H transition in the high density branch, after which they are below measurable amplitudes. In the low density branch, the ZFs reduce below measurable amplitude long before the L-H transition. The wavelength of the ZFs scales inversely with density. Zonal flows are predicted to have finite radial wavenumbers of order $k_{r,ZF} \rho_i \sim 0.1$ (where ρ_i is the ion gyroradius), but little attention has been given to dependencies of $k_{r,ZF}$.

The Experiment – Measurements were obtained during experiments in JET studying dependencies of P_{LH} . The experiment was performed in an NBI-heated plasma with toroidal field $B_\phi = 3$ T and plasma current $I_p = 2.5$ MA, with $q_{95} \approx 3.4$. In one divertor configuration using a vertically up-shifted plasma the alignment of a microwave diagnostic system [40] designed for normal-incidence correlation reflectometry measurements changed sufficiently that DBS measurements were obtained instead. This shape has a P_{LH} value that is about a factor of two higher than other configurations [39]. The NBI power was slowly ramped up to about 10 MW over 7 seconds to identify P_{LH} . The line-averaged density was varied shot-to-shot from $\langle n_e \rangle = 1.6 \times 10^{19}$ m³ to 3.1×10^{19} m³. In JET the ion and electron temperatures are equal within uncertainties even in the low density branch of the transition [41, 42]. There was a mode at about 10 kHz iden-

*See the Appendix of F. Romanelli *et al.* Proc. 25th IAEA Fusion Energy Conference 2014, Saint Petersburg, Russia

tified as the GAM [43], but it was only present during the Ohmic phase and was not of measurable amplitude during the NBI-heated L-mode or H-mode time periods. Directly after the L-H transition, the plasma enters an ELM-free H-mode with an $m=1$, $n=0$ magnetic oscillation, with frequency 1-2 kHz, at the top of the pedestal that has been named “M-mode.” [44]. In this Letter we focus on the the mean electric field and its structure.

The DBS technique [45] yields measurements of the propagation velocity of turbulent structures, v_{turb} , and density fluctuation levels. The TORBEAM beam tracing code [46] is used with the reconstructed magnetic equilibrium from EFIT and density profiles from a profile reflectometer [47] (averaged over the period of time the E_r profile is obtained) as inputs to determine the local scattering position and wavenumber. Since $v_{turb} = v_{E \times B} + v_{ph}$, if the phase velocity of the turbulence v_{ph} is small, then the measured velocity is dominated by the $v_{E \times B}$ drift and E_r can be inferred. The DBS measurements are obtained at low wavenumber, $k_{\perp} \approx 2.5 - 3.0 \text{ cm}^{-1}$. The comparison below was performed to cross-check measurement fidelity and assess the magnitude of v_{ph} .

Figure 1 compares E_r measured with DBS and with a charge exchange recombination spectroscopy (CXRS) diagnostic measuring carbon impurities, for a time window where CXRS had relatively low uncertainties. The DBS data for major radius $R < 3.75 \text{ m}$ is affected by aliasing, since the diagnostic was not originally intended for DBS measurements and was digitized at 2 MHz; aliased data is omitted. For $R > 3.75 \text{ m}$, we find good agreement for the profile shape after a radial shift has been applied. The radial shift is partially explained by a $\sim 10 \text{ cm}$ offset in the vertical position of the measurements, with the remainder likely due to $\sim 1 \text{ cm}$ uncertainty in the location of the separatrix in the reconstruction. The DBS measurements here were acquired with a single frequency source, which was adjusted by 200 MHz every 2.5 ms with a switching time of $\sim 60 \mu\text{s}$, to acquire a profile over 150 or 200 ms. The spectra for the CXRS data were averaged over 20 ms, corresponding to a time near the start of the DBS sweep. The small radial spacing between the DBS measurements enables structures smaller than the radial resolution of a single CXRS channel ($\sim 2 - 4 \text{ cm}$) to be resolved. The inset in Fig. 1 shows the polynomial fits for the individual components from CXRS and their sum. The pressure term is small due measuring an impurity. The toroidal flow dominates force balance in the core, and also contributes significantly in the E_r well region, which has been previously observed in JET [37]. The poloidal velocity would be expected to be neoclassical, following the main ion pressure gradient [48]. Profiles assuming either $v_{ph} = 0$ or $v_{ph} = v_{dia,e}$ are plotted, where $v_{dia,e} = \mathbf{B} \times \nabla P_e / (eBn_e)$ is the electron diamagnetic velocity determined from profile reflectometry and ECE; optically thin data omitted. Comparing DBS and CXRS, the data are consistent with $0 \lesssim v_{ph} \lesssim v_{dia,e}$

with best agreement in the well region for $v_{ph} \approx v_{dia,e}/2$. Later comparisons also imply a finite v_{ph} in some cases, of similar magnitude to the CXRS uncertainty. Since the kinetic profiles vary smoothly the fine scale structure in v_{turb} can be attributed to $v_{E \times B}$; however, structure in v_{ph} cannot be assessed directly from the DBS vs. CXRS comparison.

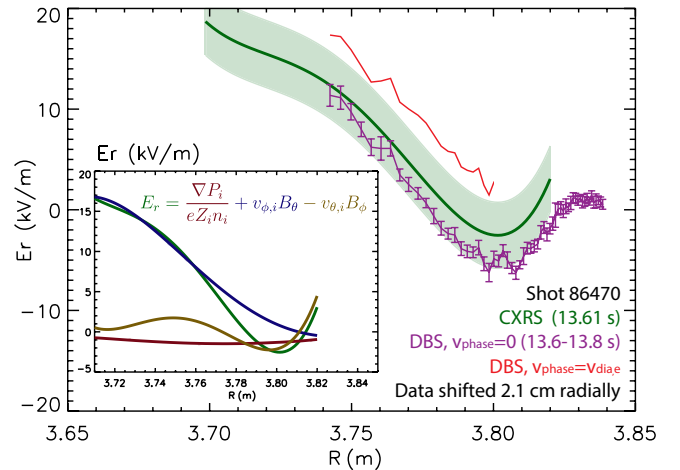


FIG. 1. (Color online) Comparison of E_r measured with CXRS (uncertainties indicated by shaded area) and DBS in L-mode. DBS data shown both assuming $v_{ph} = 0$ and $v_{ph} = v_{dia,e}$. DBS data is shifted radially by 2.1 cm. Shown inset are the the polynomial fits for each of the CXRS E_r terms and their sum.

Fine-scale spatial structure in E_r – Figure 2 shows three consecutive radial profiles of E_r inferred from DBS during a steady-state Ohmic time period. There is fine-scale structure in the profile, with static radial oscillations that persist during the 600 ms window. The measurements are highly reproducible and the spatial structures are larger than the error bars (standard deviation within each 2.5 ms step). These stationary structures are largest at the bottom of the E_r well, which corresponds to a large pressure gradient. The fine-scale structure varies with plasma conditions at fixed safety factor profile, shown in Fig. 3, so it cannot be attributed to magnetic islands that would be related to rational surfaces. Although with measurements at only one toroidal location we cannot confirm symmetry properties directly, since the structures are static in both space and time at radii with finite rotation, $n=0$ structure is strongly implied. With alternative interpretations contradicted and with measurable expectations for ZFs satisfied, we identify the fine-scale structure in E_r as zonal flows. In some shots small differences in the locations of peaks and troughs are observed, but this could be do to small changes in kinetics profiles or equilibrium, and we have no evidence for radial propagation.

The ZFs show variation with density, which is seen most clearly during the Ohmic phase. Figure 3 shows

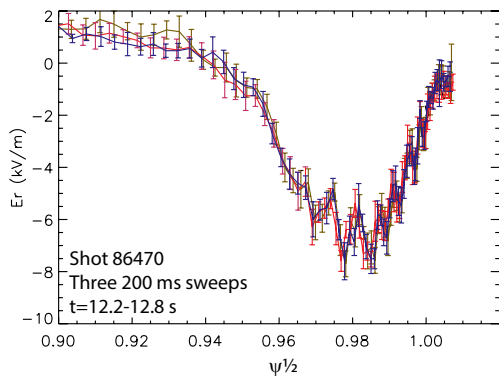


FIG. 2. (Color online) E_r profile measured with three consecutive 200 ms sweeps during a steady-state Ohmic time period.

the E_r profile and averaged density during a 200 ms steady-state Ohmic time window. As the density rises, the wavelength of the ZFs decreases and their region of existence moves outward. The width of the E_r well also decreases with density and the core E_r monotonically increases from about 0 kV/m for the lowest density to about 2.5 kV/m for the highest, at $\sqrt{\psi} \approx 0.90$, where ψ is the normalized poloidal flux.

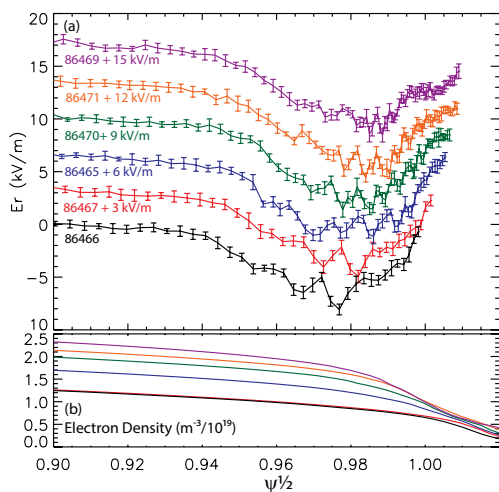


FIG. 3. (Color online) (a) Ohmic E_r profiles for six shots at different densities, $t=12.4-12.6$ s. For clarity, for each density increment the E_r profile is offset by an additional 3 kV/m (annotated). (b) Averaged n_e profile 12.4-12.6 s, from a profile reflectometer.

Parametric scaling of zonal flows – With the present limited data we cannot conclusively identify parametric scalings; however, we can compare to expectations. The amplitude, V_{ZF} , and radial wavelength, λ_{ZF} , of the ZFs are directly determined from the bottom of the E_r well in Fig. 3, and plotted as a function of the local collisionality, $\nu_* = qRv_{ii}/(v_{th,i}\epsilon^{3/2})$, in Fig. 4, where V_{ZF} is half the peak-to-peak amplitude, v_{ii} is the ion collision rate, and ϵ is the local inverse aspect ratio. There is also a

monotonic increase of λ_{ZF} with ρ_i , but ρ_i only changes by about 10%, and $k_{r,ZF}\rho_s$ spans 0.35-0.85, so the ZF wavelength is not simply changing with to keep $k_{r,ZF}\rho_i$ constant. Fig. 4 shows the scaling with collisionality, as ion collisions are expected to damp zonal flows. There is little trend for V_{ZF} , while there is a clear decrease of λ_{ZF} with ν_* ; however, ν_* values cross from banana to plateau regime, which could change the collisional regime for ZF damping [28]. The reduction of λ_{ZF} is larger than the changes to V_{ZF} , such that the zonal flow shear, $\sim V_{ZF}/\lambda_{ZF}$, increases with collisionality. This implies that arguments based only on collisional damping of ZFs, while ignoring $k_{r,ZF}$, may be misleading.

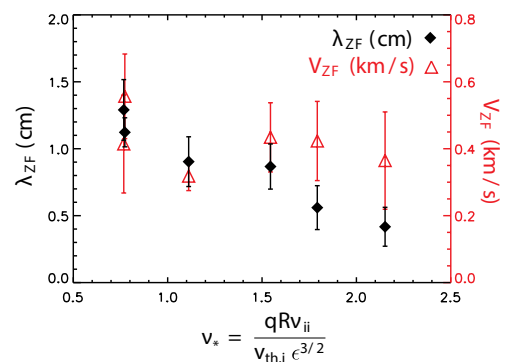


FIG. 4. (Color online) Local scaling of zonal flow radial wavelength and amplitude with collisionality.

Changes across L-H transition – Figure 5 shows the changes to E_r and density fluctuation before and after the L-H transition, identified by changes to D_α emission and the T_i profile, at several densities. The lowest density is below the minimum in the density dependence of P_{LH} , while the other two are above. Since fast dynamics are only captured for a single point, the profile during which the transition occurs is omitted; a period of unsustainable transitions in 86467 is also omitted. For several hundred milliseconds before and after the L-H transition, the E_r profile at the edge is insensitive to the slow NBI power ramp. At the lowest density, the amplitude of the ZFs is already reduced to below measurable levels during L-mode, well before the L-H transition, while there is a reduction in the ZF amplitude across the transition at high densities, observed most clearly in Fig. 5(b). Shown inset in Fig. 5(a-c) are the E_r profiles from CXRS, with polynomial fits averaged over the DBS sweep before and after the transition; different abscissa units are used due to the unknown radial offset, discussed above. At high densities we observe a clear increase in the minimum of the E_r well inferred from DBS when assuming $v_{ph} = 0$, which is not observed at low density. Although the changes are of similar magnitude to CXRS uncertainties, the CXRS E_r in both cases changes in the opposite direction to that observed with DBS, suggesting the change to the DBS profile is due to v_{ph} .

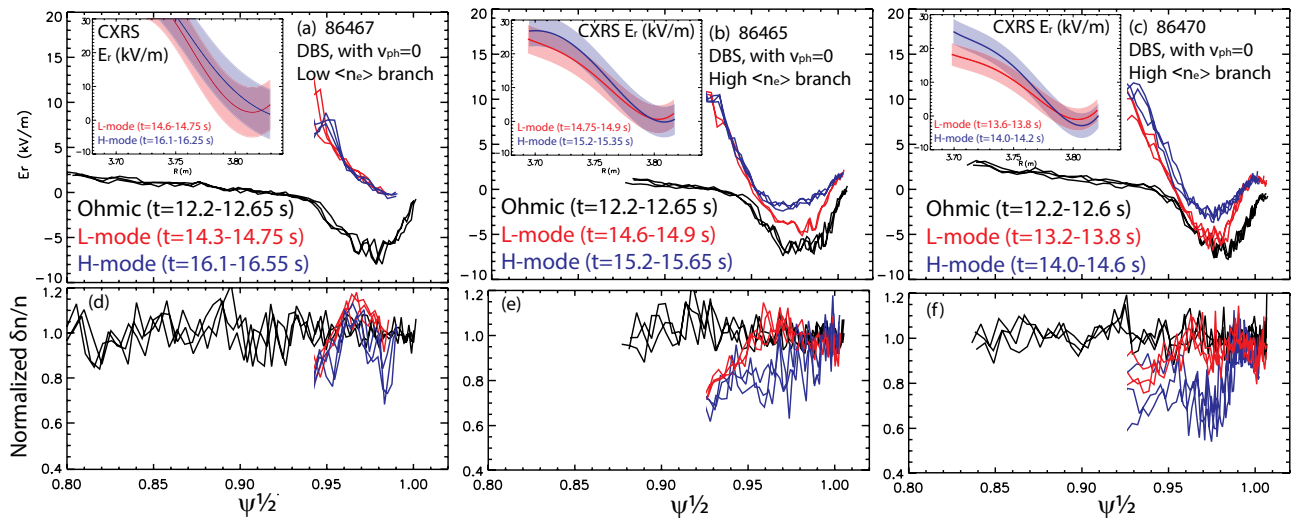


FIG. 5. (Color online) (a-c) E_r and density fluctuation (d-f) profiles for ohmic conditions and several hundred milliseconds before and after the L-H transition at 3 densities: (a,d) $\langle n_e \rangle = 1.6 \times 10^{19} \text{ m}^{-3}$, (b,e) $\langle n_e \rangle = 2.0 \times 10^{19} \text{ m}^{-3}$, and (c,f) $\langle n_e \rangle = 2.6 \times 10^{19} \text{ m}^{-3}$. Density fluctuations measured at $k_{\perp} \approx 3 \text{ cm}^{-1}$ ($k_{\perp} \rho_i \approx 0.2$) and normalized to Ohmic values.

The density fluctuation levels $\delta n/n$ at $k_{\perp} \rho_i \approx 0.2$ measured with DBS are shown in Fig. 5(d-f), normalized to a time window during the steady-state Ohmic period. For $\sqrt{\psi} < 0.95$ $\delta n/n$ falls during L-mode, as a large $E \times B$ shear is driven by the NBI. At high densities, there is a clear drop in $\delta n/n$ by 20–30% after the transition in the well region, $0.95 \lesssim \sqrt{\psi} \lesssim 0.99$. At low density, a more limited drop is observed $0.97 \lesssim \sqrt{\psi} \lesssim 0.99$, and a slight increase is observed from Ohmic to L-mode. It is notable that the drop in $\delta n/n$ across the L-H transition does *not* appear to be related to an increase in $E \times B$ shear (outside uncertainties). Since DBS measurements can be affected by non-linear saturation [49, 50], observations are a lower bound on changes to $\delta n/n$ and lack of observed change $\sqrt{\psi} \gtrsim 0.99$ could be due to saturation. These results imply that a collapse of the ZF amplitude and turbulence phase velocity, along with the fluctuation amplitude, is important for the turbulence regime in the high density branch of the L-H transition, but not in the low density branch. This is consistent with a fundamental difference in the turbulence regime in the two branches.

Conclusions – High spatial resolution DBS measurements have revealed novel insights into the development of the pedestal in JET. For the first time, fine-scale structures in the E_r profile consistent with static zonal flows have been observed in a tokamak. They appear at the bottom of the edge E_r well. This is a significant observation, implying that ZFs are what is important for development of the pedestal in JET, rather than the GAMs and LCOs observed in other experiments. The ZFs are reduced below measurable amplitude in H-mode. The different observations at high and low density also suggest a possible relation to the non-monotonic behavior of P_{LH} .

In JET there can be a well-defined E_r well even in Ohmic plasmas, instead of the well only forming after the L-H transition. For the configuration studied here, with a high P_{LH} , the NBI power required to reach the transition already results in large $E \times B$ shear and initial reduction in fluctuation amplitudes near the edge during L-mode, rather than only after the transition. These observations separate necessary conditions for sustaining the H-mode pedestal from the causes of the L-H transition and its effects, and aid in discriminating between models for the transition. For projection to larger devices like ITER, it is important to understand whether these observations are unique to the W/Be wall in JET, to the divertor configuration, to high P_{LH} with NBI heating, or whether they are universal in character, motivating further experimental and theory work.

This work has been carried out within the framework of the EUROfusion Consortium and has received funding from the Euratom research and training programme 2014-2018 under grant agreement No 633053. The views and opinions expressed herein do not necessarily reflect those of the European Commission.

* jon.hillesheim@ccfe.ac.uk

- [1] F. Wagner *et al.*, Physical Review Letters 49, 1408 (1982).
- [2] F. Wagner *et al.*, Physical Review Letters 53, 1453 (1984).
- [3] R.J. Taylor *et al.*, Physical Review Letters 63, 2365 (1989).
- [4] H. Biglari, P. H. Diamond, and P. W. Terry, Physics of Fluids B: Plasma Physics 2, 1 (1990).
- [5] R. J. Groebner, K. H. Burrell, and R. P. Seraydarian,

- Physical Review Letters 64, 3015 (1990).
- [6] K. H. Burrell, Physics of Plasmas 6, 4418 (1999).
- [7] E. J. Doyle *et al.*, Physics of Fluids B: Plasma Physics 3, 2300 (1991).
- [8] H. Matsumoto *et al.*, Plasma Physics and Controlled Fusion 34, 615 (1992).
- [9] G. R. Tynan *et al.*, Physical Review Letters 68, 3032 (1992).
- [10] G. D. Conway *et al.*, Physical Review Letters 106, 065001 (2011).
- [11] T. Estrada *et al.*, Physical Review Letters 107, 245004 (2011).
- [12] G. S. Xu *et al.*, Physical Review Letters 107, 125001 (2011).
- [13] L. Schmitz *et al.*, Physical Review Letters 108, 155002 (2012).
- [14] G. R. Tynan *et al.*, Nuclear Fusion 53, 073053 (2013).
- [15] T. Kobayashi *et al.*, Physical Review Letters 111, 035002 (2013).
- [16] K. H. Burrell *et al.*, Plasma Physics and Controlled Fusion 34, 1859 (1992).
- [17] J. W. Connor and H. R. Wilson, Plasma Physics and Controlled Fusion 42, R1 (2000).
- [18] E. J. Doyle *et al.*, Nuclear Fusion 47, S18 (2007).
- [19] W. Fundamenski *et al.*, Nuclear Fusion 52, 062003 (2012).
- [20] E. R. Solano and R. D. Hazeltine, Nuclear Fusion 52, 114017 (2012).
- [21] K. Miki *et al.*, Physical Review Letters 110, 195002 (2013).
- [22] C. Bourdelle *et al.*, Nuclear Fusion 54, 022001 (2014).
- [23] G. M. Staebler and R. J. Groebner, Plasma Physics and Controlled Fusion 57, 014025 (2015).
- [24] X. Wu *et al.*, Nuclear Fusion 55, 053029 (2015).
- [25] M. N. Rosenbluth and F. L. Hinton, Physical Review Letters 80, 724 (1998).
- [26] A. Fujisawa *et al.*, Physical Review Letters 93, 165002 (2004).
- [27] D. K. Gupta *et al.*, Physical Review Letters 97, 125002 (2006).
- [28] P. H. Diamond *et al.*, Plasma Physics and Controlled Fusion 47, R35 (2005).
- [29] B. Scott, Physics Letters A 320, 53 (2003).
- [30] G. Dif-Pradalier *et al.*, Physical Review Letters 114, 085004 (2015).
- [31] S. J. Fielding *et al.*, Plasma Physics and Controlled Fusion 38, 1091 (1996).
- [32] T. N. Carlstrom and R. J. Groebner, Physics of Plasmas 3, 1867 (1996).
- [33] L. D. Horton *et al.*, Proc. 26th EPS Conf. on Controlled Fusion and Plasma Physics, Maastricht, The Netherlands (1999).
- [34] Y. Andrew *et al.*, Plasma Physics and Controlled Fusion 48, 479 (2006).
- [35] F. Ryter *et al.*, Nuclear Fusion 49, 062003 (2009).
- [36] Y. Ma *et al.*, Nuclear Fusion 52, 023010 (2012).
- [37] C. F. Maggi *et al.*, Nuclear Fusion 54, 023007 (2014).
- [38] F. Ryter *et al.*, Nuclear Fusion 54, 083003 (2014).
- [39] H. Meyer *et al.*, Proc. 41st European Physics Society Conference on Plasma Physics, P1.013 (2014).
- [40] A. Sirinelli *et al.*, Proc. 11th Intl. Reflectometry Workshop - IRW11, Palaiseau, France (2013).
- [41] E. Delabie *et al.*, Proc. 25th IAEA Fusion Energy Conference, Saint Petersburg, Russia, EX/P5 (2014).
- [42] E. Delabie *et al.*, Proc. 42nd European Physics Society Conference on Plasma Physics, O3.113 (2015).
- [43] C. Silva *et al.*, Proc. 42nd European Physics Society Conference on Plasma Physics, O3.114 (2015).
- [44] E. R. Solano *et al.*, Proc. 40th European Physics Society Conference on Plasma Physics, P4.111 (2013).
- [45] M. Hirsch and E. Holzhauser, Plasma Physics and Controlled Fusion 46, 593 (2004).
- [46] E. Poli, A. G. Peeters, and G. V. Pereverzev, Computer Physics Communications 136, 90 (2001).
- [47] A. Sirinelli *et al.*, Review of Scientific Instruments 81, 10D939 (2010).
- [48] E. Viezzer *et al.*, Nuclear Fusion 54, 012003 (2014).
- [49] E. Z. Gusakov, A. V. Surkov, and A. Y. Popov, Plasma Physics and Controlled Fusion 47, 959 (2005).
- [50] U. Stroth *et al.*, Nuclear Fusion 55, 083027 (2015).